Heliyon 10 (2024) e29228

Contents lists available at ScienceDirect

Heliyon

journal homepage: www.cell.com/heliyon

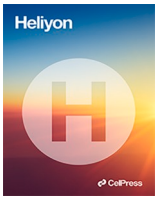

Research article

Thermal and solutal transport by Cattaneo-Christov model for the magnetohydrodynamic Williamson fluid with joule heating and heat source/sink

T. Salahuddin, Muhammad Awais *

Department of Mathematics, Mirpur University of Science and Technology, (MUST), 10250, Pakistan

ARTICLE INFO

Keywords:
Variable viscosity
Williamson fluid
Magnetic field
Stretching sheet
Cattaneo-Christov
Heat source/sink
Adams-Milne (predictor-corrector method)

ABSTRACT

This article scrutinizes the 2-dimensional and boundary layer flow of magnetohydrodynamic Williamson fluid flowing on a stretchable surface with variable viscosity. The thermal and solutal rates are examined through the Cattaneo-Christov model with Joule heating, heat source/sink, and chemical reaction. The authors are motivated to conduct this study because of its practical and scientific significance in various processes, including polymer processing, textile industries, food industries, solar energy, biomedical science, wind turbine blades, oil spill clean-up, metal rolling, and forging. With the mentioned assumptions, the partial differential equations are achieved by using the basic governing laws, including momentum law, energy law, and concentration law. This non-linear system of equations is transmuted into ordinary differential equations by taking similarity transformations. The main novelty behind the conduction of this work is the numerical technique, namely the 'Adams-Milne (Predictor-Corrector)' method along with the Runge-Kutta technique on Matlab software, which has not previously been studied by any researcher in the literature. The analytical solution of the determined equations is not possible due to their highly non-linear nature; therefore the multistep numerical method namely the 'Adams-Milne (Predictor-Corrector)' method, along with the Runge-Kutta technique is used to determine the numerical results. The outcomes are noted due to numerous parameters for velocity, temperature, and concentration profiles. The explanation of graphical and numerical results is discussed here. The graphical impression of the Williamson parameter reveals that the velocity and temperature curves diminish for higher inputs of this parameter. The movement of fluid shows the declining behavior for the Hartmann number and viscosity parameter. The solutal and thermal findings due to Cattaneo-Christov heat and mass relaxation coefficients mark the reducing behaviour in respective field. The rise in reaction coefficient decreases the mass distribution. The analyses of comparison of results are also presented here.

1. Introduction

Non-Newtonian fluids are frequently used in engineering and medicine because of their dynamical properties. An extensive variety of industrial and biological uses, including the production of food, drilling operations, and improving oil recovery, are available for non-Newtonian fluids with shear-thinning behavior. The rheological properties of fluids are still not adequately described by the

* Corresponding author.
E-mail address: awaisjanjua919@gmail.com (M. Awais).

https://doi.org/10.1016/j.heliyon.2024.e29228
Received 31 October 2022; Received in revised form 28 March 2024; Accepted 3 April 2024
Available online 4 April 2024

Navier-Stokes equations. Several rheological models, including the Power law, Sutterby, Jeffery, Casson, Carreau-Yaseuda, Maxwell, and Sisko fluid models, have been developed to address this issue and recently Williamson fluid took the attention. Williamson created a model equation in 1929 that outlined the characteristics of rheological fluids. Nadeem et al. [1] scrutinized the 2D Williamson fluid flowing on the stretchy sheet. Malik et al. [2] solved the numerical solutions of the non-Newtonian (Williamson fluid) with a stagnation point flowing on the stretchy cylinder. Salahuddin et al. [3] determined the Williamson fluid behavior that is passing on the stretchy sheet, whereas the solutal and thermal transport processes are also determined with the viscous dissipation and C–C model. Ramamoorthy and Pallavarapu [4] determined the Hall effects for the 3-dimensional Williamson fluid passed over a stretched surface and revealed that by increasing the fluid parameter the velocity declined. Ahmed et al. [5] computed the thermal transmission processes of magnetohydrodynamic Williamson flow with variable conductivity and the fluid is passing on the porous stretchy surface. The heat transmission in Williamson fluid in the presence of C–C flux passed on the porous material was examined by Nawaz et al. [6]. Waqas et al. [7] discussed Fourier's theory and convection impact on Williamson fluid flow with thermal generation. Meenakumari et al. [8] calculated the magnetohydrodynamic and radiation impacts on the Williamson fluid flowing over the stretchy surface. Salahuddin [9] inspected the physical characteristics of an electrically conducting boundary layer with the consequences of chemical reactions and solar radiation over the stretchable surface of Williamson fluid. The impression of heterogeneous-homogeneous reactions and the flow with heat transfer caused by the motion of Williamson fluid was examined numerically by Hamid [10].

Magnetohydrodynamics (MHD) is an area of fluid dynamics dealing with heat transfer. On the other hand, it is the dynamics of a fluid that is conducting current and subjected to a magnetic field. Theoretically, a drag force recognized as the Lorentz force may be experienced by a fluid moving through a magnetic field, and this force is the source of rising the fluid's concentration and temperature. The study of the dynamical interactions among fluids and magnetic fields is called magnetohydrodynamics (MHD). There are several applications for MHD in the polymer industry, including optical fibre filters, crystal formation, magnetohydrodynamic generators, and plastic stretching sheet. Awais and Salahuddin [11] scrutinized the magnetohydrodynamic flow of cross fluid with varying characteristics and passing on the parabolic surface. Reddy and Maddileti [12] analyzed the Joule parameter and MHD Casson nanofluid flowing over the stretched plate. Shamshuddin et al. [13] investigated a computational study by assuming the effects of Hall current, energy dissipation and joule heating for the 2-D power-law fluid that is moving on the exponentially stretchy sheet. Swain et al. [14] scrutinized the thermal transport of MHD flow through a stretched sheet encased in a porous medium, which is affected by joule heating. Sharma and Gandhi [15] presented the MHD convective flow across the stretchy surface with the Darcy-Forchheimer medium and determined the impacts of joule heating and thermal source/sink.

The impression of variable viscosity on flow and thermal transmission has grown more importance due to its technical utilization including the extraction of crude oil, geothermal systems, equipment lubrication, etc. Particularly in machines, the bearings get heated up from friction and need to be lubricated to work properly. This frictional temperature may impact the viscosity of the lubricant. It's important to note down how viscosity changes with temperature to calculate the physical behaviour of this type of problem. Devi and Prakash [16] considered the variable viscosity of hydromagnetic flow, which is passed on the stretchy surface. Fatunmbi et al. [17] modelled the equations of MHD micropolar fluid with variable viscosity and fluid flowing on the elongating surface. This study illustrates that the motion of fluids decreases with variation in the viscosity coefficient. Sobamowo and Akinshilo [18] considered the regular perturbation approach to analyse the pipe flow, heat transmission properties, and entropy formation in a fluid with varying viscosity. Reddy et al. [19] investigated numerically the impact of viscosity change on the formation of entropy in Reiner-Rivlin fluid moving on an infinite vertical plate, and results were obtained via the Crank-Nicolson method.

The Cattaneo-Christov model incorporates a finite thermal wave speed and a time delay in heat conduction, which is significant and has found uses in many areas of science and engineering because of its capacity to give a more accurate description of heat transmission in certain circumstances. The researcher used this model because of its uses in thermal insulators, semiconductor physics, nanoscale heat transport, biomedical engineering, energy storage, nuclear reactors, electrical cooling, and many more industrial applications. Fourier was the first to study the law of heat conduction [20]. By using the C–C theory, Hayat et al. [21] illustrated the heat transmission properties of rotating discs with varied thickness. Salahuddin and Awais [22] conducted a problem based on the C–C theory for the motion of stress fluid through variable viscosity and passed over the sensory squeezing channel. The remarks indicate that the solutal and heat fields decline due to the use of the Cattaneo-Christov theory. Reddy et al. [23] inspected the C–C theory for nanofluid flowing on a porous stretchy surface with chemical reaction. The Cattaneo-Christov-Christovs considered by Khan et al. [24] to investigate the Maxwell fluid that is passing through the stretched cylinder. Awais and Salahuddin [25] determined the convective flow with variable viscosity of a non-Newtonian fluid that is moving on the paraboloid surface with the C–C theory. The impact of C–C theory in the transferal process of mass and heat flow in cross fluid was scrutinized by Salahuddin et al. [26]. This study reveals that the solutal and thermal rates decline due to temperature and concentration relaxation coefficients. Mallawi et al. [27] examined the transfer of energy and mass with double stratification, thermal radiation, and C–C theory in terms of non-Newtonian fluid passing over the Riga plate. Both thermal and solutal stratification coefficients enhance the respective fields. Reddy et al. [28] presented a model of study using the Cattaneo-Christov theory for the flow of nanofluid on the sheet with porosity.

One must use a temperature-dependent heat source or sink because it has a significant influence on the heat transmission characteristics when there is a significant difference between the surface and the upstream fluid. A number of physical issues make it crucial to examine heat generation or absorption in flowing fluids. In electronic chips, nuclear reactors, and semiconductor wafers, the temperature distribution may change as a result of heat generating effects. While exact heat generation or absorption modelling is fairly complicated, certain mathematical models can explain its typical behavior in physical scenarios. Thumma et al. [29] studied numerically the thermal source or sink for the dissipative MHD nanofluid flowing on the stretchable sheet. Mahabaleshwar et al. [30] determined the thermal transport by assuming the CNT nanofluids passing on the shrinking or stretching surface with thermal source or sink. Ajaykumar et al. [31] inspected the impacts of heat source or sink and dissipation on the motion and transmission of heat in a

MHD fluid flowing on a moving flat surface. Ragupathi and Prakash [32] investigated the linear and nonlinear radiation impressions on the nanofluids across a rotating porous disc with a heat source or sink. Noor and Shafie [33] determined the MHD squeezing flow of Jeffery fluid by embedding the hybrid nanofluid, and thermal analysis was inspected by heat source and sink. Some related studies are cited in Refs. [34–39].

The novelty of this work is that we consider the variable viscosity of the 2D boundary layer and the magnetohydrodynamic Williamson fluid flowing on the stretched sheet. Here we have also examined heat and mass transport by assuming the chemical reaction, the Cattaneo-Christov theory, joule heating and heat source/sink. The novelty of this work is that we used the Adams-Milne (Predictor-Corrector) method along with the Runge-Kutta technique, and this type of multistep method was not taken by any researcher in the past. The basic conservation laws are implemented to develop the governing partial differential equations, and the appropriate transformations renovated these equations into the ordinary differential equations. The numerical solutions are determined by using the Adams-Milne Predictor Corrector formula along with the RK technique. The outcomes of the emerging parameters are discussed in a numerical and graphical way.

2. Problem formulation

Considering a 2-D incompressible magnetohydrodynamic boundary layer Williamson fluid that is flowing on the surface coincides with the plane at $y = 0,$ and the fluid is restricted to be flowing on $y > 0$. The thermal and solutal rates are scrutinized by using the Cattaneo-Christov theory along with joule heating and chemical reaction. The physical interpretation in the form of flow geometry is shown in Fig. 1.

2.1. Governing equations

The basic governing equations (continuity, momentum, temperature and concentration) in terms of the considered assumption are

$$\partial_{x^*} u^* + \partial_{y^*} v^* = 0, \tag{1}$$

$$\rho\left(u^* \partial_x u^* + v^* \partial_y u^*\right) = -\partial_{x^*} \mathrm{p}^* + \partial_{x^*} \tau^*_{x^* x^*} + \partial_{y^*} \tau^*_{x^* y^*} + \rho \mathrm{b}^*_x, \tag{2}$$

$$\rho\left(u^* \partial_{x^*} v^* + v^* \partial_{y^*} v^*\right) = -\partial_{y^*} p^* + \partial_{x^*} \tau^*_{y^* x^*} + \partial_{y^*} \tau^*_{y^* y^*} + \rho \mathrm{b}^*_y, \tag{3}$$

$$\rho C_p \left(u^* \partial_{x^*} T^* + v^* \partial_{y^*} T^*\right) = -\nabla.\mathrm{G}^*, \tag{4}$$

$$\left(u^* \partial_{x^*} C^* + v^* \partial_{y^*} C^*\right) = -\nabla.\mathrm{H}^*. \tag{5}$$

here (x^*, y^*) are the cartesian coordinate axis, (u^*, v^*) are the components of velocity, p^* symbolize as pressure, (C^*, T^*) be the concentration field and temperature field, whereas (C^*_∞, T^*_∞) magnifies as the upstream concentration and temperature, ρ denoted as density, τ^* shows the stress tensor, (b^*_x, b^*_y) be the body forces and C_p symbolized as specific heat. The model equations of Cattaneo-Christov flow theory are given as [3,22],

$$G^* + \lambda_1((\nabla.V^*) - G^*.\nabla V^* G^* + V^*.\nabla G^*) = -K\nabla T^*, \tag{6}$$

$$H^* + \lambda_2((\nabla.V^*)H^* - H^*.\nabla V^* + V^*.\nabla H^*) = -D\nabla C^*, \tag{7}$$

here the mass and heat relaxation time are denoted as λ_2 and λ_1. In case of steady flow, $\nabla.V^* = 0,$ then the above equations reduces as,

$$G^* + \lambda_1(V^*.\nabla G^* - G^*.\nabla V^*) = -K\nabla T^*, \tag{8}$$

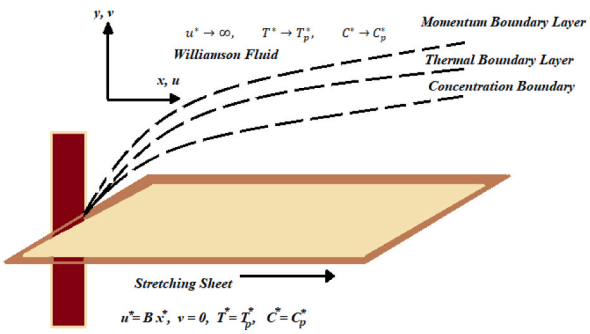

Fig. 1. Physical geometry of fluid flow.

$$H^* + \lambda_2(V^*.\nabla H^* - H^*.\nabla V^*) = -D\nabla C^*, \tag{9}$$

Implementing the boundary layer approximation, then the governing equations takes the following form [3,40,41].

$$\begin{aligned}\rho\left(u^*\partial_{x^*}u^* + v^*\partial_{y^*}u^*\right) &= \mu^*\left(\partial_{y^*y^*}u^*\right) + \left(\partial_{y^*}\mu^*\right)\left(\partial_{y^*}u^*\right) + \left(\partial_{y^*}\mu^*\right)\left(\Gamma/2\right)\left(\partial_{y^*}u^*\right)^2 \\ &+\sqrt{2}\mu^*\Gamma\left(\partial_{y^*}u^*\right)\left(\partial_{y^*y^*}u^*\right) - \sigma^*B_\circ^*u,\end{aligned} \tag{10}$$

$$\rho C_p\left(u^*\partial_{x^*}T^* + v^*\partial_{y^*}T^*\right) - \lambda_1\varphi_1 = K\left(\partial_{y^*y^*}T^*\right) + \sigma^*B_\circ^*u^2 + Q^{'''}, \tag{11}$$

$$\left(u^*\partial_{x^*}C^* + v^*\partial_{y^*}C^*\right) - \lambda_1\varphi_2 = D\left(\partial_{y^*y^*}C^*\right) - \kappa\left(C^* - C_\infty^*\right), \tag{12}$$

now defininig φ_1 and φ_2 as [3,22,24]

$$\varphi_1 = \begin{bmatrix} u^*(\partial_{x^*}u^*)(\partial_{x^*}T^*) + v^*\left(\partial_{y^*}v^*\right)\left(\partial_{y^*}T^*\right) + u^*(\partial_{x^*}v^*)\left(\partial_{y^*}T^*\right) + v^*\left(\partial_{y^*}u^*\right)(\partial_{x^*}T^*) \\ +2u^*v^*\left(\partial_{x^*y^*}T^*\right) + u^{*^2}(\partial_{x^*x^*}T^*) + v^{*^2}\left(\partial_{y^*y^*}T^*\right) \end{bmatrix}, \tag{13}$$

$$\varphi_2 = \begin{bmatrix} u^*(\partial_{x^*}u^*)(\partial_{x^*}C^*) + v^*\left(\partial_{y^*}v^*\right)\left(\partial_{y^*}C^*\right) + u^*(\partial_{x^*}v^*)\left(\partial_{y^*}C^*\right) + v^*\left(\partial_{y^*}u^*\right)(\partial_{x^*}C^*) \\ +2u^*v^*\left(\partial_{x^*y^*}C^*\right) + u^{*^2}(\partial_{x^*x^*}C^*) + v^{*^2}\left(\partial_{y^*y^*}C^*\right) \end{bmatrix}. \tag{14}$$

in thermodynamics and engineering, the words "heat source" and "heat sink" are used to explain the systems that either emit heat (source) or absorb heat (sink). This term occurs in temperature equation [42].

$$Q^{'''} = \frac{KU_w}{xv^*}\left[a^*\left(T_p^* - T_\infty^*\right)F'(\eta) + b^*\left(T^* - T_\infty^*\right)\right], \tag{15}$$

here a^* and b^* are the parameters of internal heat source/sink.

2.2. Boundary conditions

The boundary conditions are [3,43].

$$\begin{aligned} &u^* = Bx^*, v^* = 0, T^* = T_p^*, C^* = C_p^*, at \quad y^* = 0, \\ &u^* \to 0, T^* = T_\infty^*, C^* = C_\infty^*, as \quad y^* \to 0. \end{aligned} \tag{16}$$

here B is the stretching parameter.

2.3. Transformations

Similarity variables are essential in dimensionalizing the flow equations and it is a technique used for relating physical parameters and variables in a problem. The flow system is transmuted into non-dimensional form by considering the appropriate transformations [44–46].

$$\begin{aligned} &u^* = Bx^*F'(\eta), v^* = -\sqrt{Bv^*}F(\eta), T^* = T_\infty^* + \left(T_p^* - T_\infty^*\right)\Theta, \\ &C^* = C_\infty^* + \left(C_p^* - C_\infty^*\right)\Phi, \eta = \sqrt{B/v^*}y^*. \end{aligned} \tag{17}$$

The utilization of transformations in the partial differential equations alters the governing model into dimensionless form.

$$\begin{aligned}\left(\frac{\Theta_a + \Theta}{\Theta_a}\right)F'''(\eta) + \left(\frac{1}{\Theta_a}\right)\Theta'(\eta)F''(\eta) + \left(\frac{1}{\Theta_a}\right)\Theta'(\eta)\frac{W_e}{2}(F''(\eta))^2 \\ +W_e\left(\frac{\Theta_a + \Theta}{\Theta_a}\right)F''(\eta)F'''(\eta) - H_aF'(\eta) = 0,\end{aligned} \tag{18}$$

$$\begin{aligned}\Theta''(\eta) + P_rF(\eta)\Theta'(\eta) - \chi_1P_r\left[F(\eta)F'(\eta)\Theta'(\eta) + F^2(\eta)\Theta''(\eta)\right] \\ +P_rE_cH_a(F'(\eta))^2 + \frac{1}{\left(1 + \frac{\Theta(\eta)}{\Theta_a}\right)}\left[a^*F'(\eta) + b^*\Theta\right],\end{aligned} \tag{19}$$

$$\Phi''(\eta) - S_cF'(\eta)\Phi(\eta) - \chi_2S_c\left[F(\eta)F'(\eta)\Phi'(\eta) + (F(\eta))^2\Phi''\right] - S_c\delta\Phi = 0, \tag{20}$$

the boundary conditions are

$$F(\eta)=1, F^{'}(\eta)=1, \Theta(\eta)=1, \Phi(\eta)=1, \text{at} \quad \eta=0, \\ F^{'}(\infty)=0, \Theta(\infty)=0, \Phi(\infty)=0, \tag{21}$$

here Θ_a signifies as the viscosity parameter, W_e represents the Weissenberg number, H_a demoted as the Hartmann number, P_r symbolizes as the Prandtl number, χ_1 thermal relaxation coefficient, E_c is Eckert number, χ_2 solutal relaxation coefficient, S_c symbolized as the Schmidt number and δ is the reaction coefficient. These parameters are

$$W_e = x^*\Gamma\sqrt{\frac{2B^3}{\upsilon^*}}, \quad E_c = \frac{U_w^2}{C_p\left(T_p^*-T_\infty^*\right)} P_r = \frac{C_p\mu^*}{K}, H_a = \frac{\sigma^* B_\circ^*}{\rho B}, S_c = \frac{\upsilon^*}{D}, \chi_1 = \lambda_1 B, \\ \chi_2 = \lambda_2 B, \delta = \frac{\kappa}{B}. \tag{22}$$

2.4. Physical quantities

The effects of physical quantities including friction factor, Nusselt number and Sherwood number are discussed here.

$$\overline{C}_{f^*} = \frac{\tau_w}{\rho U_w^2}, \overline{N}_{ux^*} = \frac{x^*\overline{q}_w}{K\left(T_p^*-T_\infty^*\right)}, \overline{S}_{hx^*} = \frac{x^*\overline{q}_m}{D\left(C_p^*-C_\infty^*\right)}, \tag{23}$$

the dimensional form of these physical quantities are

$$\sqrt{\mathrm{R}_{ex}}\overline{C}_{f^*} = \left(1+\frac{\Theta}{\Theta_a}\right)\left[F^{''}+\frac{W_e}{2}(F^{''})^2\right]_{\eta=0}, \\ \frac{\overline{N}_{ux^*}}{\sqrt{\mathrm{R}_{ex}}} = -\Theta^{'}|_{\eta=0}, \\ \frac{S_{hx^*}}{\sqrt{\mathrm{R}_{ex}}} = -\Phi^{'}|_{\eta=0}. \tag{24}$$

here the dimensionless number is Reynolds number which is defined as $\mathrm{R}_{ex} = \frac{Bx^{*2}}{\upsilon^*}$.

3. Numerical technique

The ODEs (18–20) along with boundary conditions (21) are highly non-linear system of equations and we adopted Adam-Milne Predictor Corrector method in order to get the numerical results. By using the Adams-Milne method, we have to convert the primary equations into 1st-order form, and then these equations are solved in Matlab software by using the Adam-Milne method along with the root finding secant method. Adams-Milne (Predictor-Corrector) approaches work on the fundamental premise that past solution values can be used to examine further solution values (Predictor step), and that these predicted values can subsequently be used to correct estimations (corrector step). These techniques make use of both previous and current data to produce precise results. We summarized the results through graphs and discussion and validation of the results are also placed here.

The procedure for finding the solution through the Adams-Milne (Predictor-Corrector) method is that we must convert our system of governing equations into first-order form by applying the transformations. These transformations are

$$y(1)=\mathrm{F}(\eta), \mathrm{y}(2)=\mathrm{F}^{'}(\eta), \mathrm{y}(3)=\mathrm{F}^{''}(\eta), \mathrm{y}^{'}(3)=\mathrm{F}^{'''}(\eta), \mathrm{y}(4)=\Theta(\eta), \mathrm{y}(5)=\Theta^{'}(\eta), \\ y^{'}(5)=\Theta^{''}(\eta), y(6)=\Phi(\eta), y(7)=\Phi^{'}(\eta), y^{'}(7)=\Phi^{''}(\eta). \tag{25}$$

The transmuted forms of equations are

$$y^{'}(3) = -\frac{1}{\left(1+\frac{y(4)}{\Theta_a}\right)(1+W_e y(3))}\left[\frac{1}{\Theta_a}\left\{y(3)\mathrm{y}(5)+\frac{W_e}{2}\mathrm{y}(5)(\mathrm{y}(3))^2\right\}+H_a\, y(2)\right], \tag{26}$$

$$y^{'}(5) = \frac{1}{1-\chi_1 P_r(y(1))^2}\begin{bmatrix} -P_r\left(y(1)\mathrm{y}(5)+\chi_1 y(1)\mathrm{y}(2)\mathrm{y}(5)-E_c H_a\left(y(1)^2\right)\right) \\ -\frac{1}{\left(1+\frac{y(4)}{\Theta_a}\right)}\{a^* y(2)+b^* y(4)\} \end{bmatrix}, \tag{27}$$

$$y^{'}(7) = \frac{1}{1-\chi_2 S_c(y(1))^2}[-S_c y(1)\mathrm{y}(7)+S_c y(1)\mathrm{y}(2)\mathrm{y}(7)+S_c\delta y(6)], \tag{28}$$

the boundary conditions are

$$\begin{aligned} &y(1)=0, y(2)=1, y(4)=1, y(6)=1, at \quad \eta=0, \\ &y(2)\to 0, y(4)\to 0, y(6)\to 0, at \quad \eta\to\infty. \end{aligned} \tag{29}$$

We first calculate the initial values using the Runge-Kutta fourth order method because the numerical technique being studied is a multistep method known as Predictor-Corrector. Next, we must apply the fourth order Adams predictor formula which is

$$y_{j+1,r}=y_{j-3}+\left(\frac{4}{3}\right)h\left[2F_j-F_{j-1}+2F_{j-2}\right], \tag{30}$$

The corrector formula of Adams-Milne method is

$$y_{j+1,c}=y_{j-1}+\left(\frac{1}{3}\right)h\left[F_{j+1}+4F_j+F_{j-1}\right], \tag{31}$$

The values of (F_1, F_2, F_3) are calculated with fourth order Runge-Kutta method and (F_4) is examined with the Adams-Bashforth scheme. The general form of Runge-Kutta fourth order method is

$$y_{j+1}=y_j+\frac{1}{6}\left[\widehat{K}_1+2\widehat{K}_2+2\widehat{K}_3+\widehat{K}_4\right], \tag{32}$$

where

$$\begin{aligned} \widehat{K}_1 &= hF\left(x_j, y_j\right), \\ \widehat{K}_2 &= hF\left(x_j+\left(\frac{1}{2}\right)\mathrm{h}, y_j+\left(\frac{1}{2}\right)k_1\right), \\ \widehat{K}_3 &= hF\left(x_j+\left(\frac{1}{2}\right)\mathrm{h}, y_j+\left(\frac{1}{2}\right)k_2\right), \\ \widehat{K}_2 &= hF\left(x_j+\mathrm{h}, y_j+k_3\right). \end{aligned} \tag{33}$$

The calculated values with the R–K method are placed into the Adams-Milne Predictor and Corrector formulas to get the desired results. The final results of the velocity, temperature and concentration equations are calculated from the boundary conditions. If the difference is less than a small number $\varepsilon = 0.01$, then we get our desired results. But if the difference is not less than ε, then we again use the same procedure and get second result. The second results is also matched with the small number ε. Now if we get the difference less than ε, then we obtained the final result. If again the difference is never less than small number ε. Then we use the secant method to improve the initial guess. The similar procedure is repeated until it satisfies the boundary conditions. This is a fourth order method and the truncation error is of fourth order.

4. Results and discussions

The study of magnetohydrodynamic Williamson fluid passing on a stretchable sheet with variable viscosity is investigated here. The solutal and thermal transference processes are scrutinized by considering the Cattaneo-Christov model, heat source or sink and chemical reaction. The results are determined by using the Adams-Milne method on Matlab software and the graphical form of the results is placed in this section.

Table 1 exhibits the numerical determinations of $\overline{N}_{ux^*}$ due to making the variation in the Prandtl number P_r, thermal relaxation coefficient χ_1, Hartmann number H_a, Eckert number E_c and viscosity coefficient Θ_a. The increment happens in Nusselt number $\overline{N}_{ux^*}$ by making the variation in Prandtl number P_r and thermal relaxation coefficient χ_1. The decrement in Nusselt number and heat transfer rate is noted due to varying the Hartmann number, viscosity coefficient and Eckert number. Table 2 reveals the numerical

Table 1
Numerical determinations of $\overline{N}_{ux^*}$ due to making the variation in the Prandtl number P_r, thermal relaxation coefficient χ_1, Hartmann number H_a, Eckert number E_c and viscosity coefficient Θ_a.

P_r	χ_1	H_a	E_c	Θ_a	$\overline{N}_{ux^*}$
1.5	0.1	0.1	0.2	0.1	1.1985
2.0					1.5147
2.5					1.7488
	0.2				1.2001
	0.3				1.2722
		0.2			1.1855
		0.3			1.1729
			0.2		1.1962
			0.3		1.1940
				0.2	1.1967
				0.3	1.1955

determinations of $\overline{S}_{hx^*}$ due to making the variation in the Schmidt number S_c and solutal relaxation coefficient χ_2. Both the parameters are the sources of decrement in the Sherwood number $\overline{S}_{hx^*}$.

4.1. Validation of results

For the validation of numerical results, we have taken the comparison analysis of friction coefficient $\overline{C}_{f^*}$ by varying the inputs of Williamson coefficient and assuming the other parameter to be zero with the past publish article and outcomes are exhibited in Table 3. The outcome shows similar behaviour with past results.

4.2. Velocity region

Here the discussion comprises the impression of emerging parameters on the velocity region. The sketch placed in Fig. (2a) explains the results of viscosity parameter Θ_a on the velocity region and we inspected that the decrement in the fluid movement is happening due to viscosity coefficient Θ_a. The fact is that the velocity distribution can vary based on the precise flow circumstances and fluid characteristics, a higher viscosity generally leads to a steeper velocity gradient due to the highly viscous fluid. The applied magnetic field on the fluid marks huge impression on the velocity region and the result is revealed in Fig. (2b). The determined finding indicates that the Hartmann number H_a oppose the movement of fluid and drops the velocity curve. The influence of the magnetic field grows stronger as by increasing its strength. The electrically conducting fluid experiences a Lorentz force from the magnetic field, which causes "Hartmann layers" to form close to the surface. The Hartmann layers decrements the fluid velocity due to magnetic dampening. The sketch placed in Fig. (2c) illustrates the outputs of velocity region by varying the Weissenberg number W_e. The determining outcomes illustrates that the Weissenberg number W_e marks the declining impression on the velocity curve. Physically, these findings are occurred because Weissenberg number W_e has direct impact with the time relaxation and in higher time relaxation, the fluid needs further time to achieve the final position. Therefore the velocity curve declines due to W_e.

4.3. Temperature profile

The graphical dependency of viscosity coefficient Θ_a on the temperature region is revealed in Fig. (3a). The finding illustrated that the temperature curve enhances by producing the viscosity coefficient Θ_a. High viscosity of fluid provides a large amount of deformation resistance. The fluid friction generates a significant amount of heat energy. Due to the alteration of mechanical energy into thermal energy, the temperature distribution exhibits noticeable differences, with notably higher temperatures. Therefore the curve upsurges due to Θ_a. The outcome of Hartmann number H_a in the thermal region is placed in Fig. (3b). The sketch explains the incrementing behaviour of Hartmann number H_a. Physically, Electromagnetic forces are dominant in higher Hartmann number, therefore upsurge in temperature results from the varying inputs of H_a. The graph revealed in Fig. (3c) is plotted to determine the graphical outputs of thermal relaxation parameter χ_1 on the temperature region. The determined outcomes show that the χ_1 lowering the temperature curve. When the magnitude of thermal relaxation coefficient is high, the material reacts to temperature changes slowly. The temperature distribution transitions slowly, and it takes higher time for it to achieve a steady state. The deviation in Weissenberg number W_e has significant impact on the temperature region and graphical behaviour is shown in Fig. (3d). The findings indicated that the temperature region increases due to Weissenberg number. There is significant elastic deformation when the Weissenberg number is large. Due to mechanical work, the material deforms prominently and produces a significant amount of heat. Therefore the temperature upsurges due to W_e. The deviation of heat source and sink coefficient upon the thermal region is placed in Fig. 3(e and f). Both the parameters make the enhancement in the temperature curve.

4.4. Concentration profile

The impacts of parameters on mass profile are revealed in this subsection. Fig. (4a) depicts the mass flux impression for various inputs of the Schmidt number S_c. The result demonstrates that the mass curve decreases as the Schmidt number increases in magnitude. Since the Schmidt number is the reverse of that of solutal diffusion, a loss in mass diffusion corresponds to a decrease in mass rate by upsurge the Schmidt number S_c. The variation of mass rate for different magnitudes of solutal relaxation coefficient χ_2 is shown in Fig. (4b). The observations show that the mass distribution decreases when the solutal relaxation time coefficient χ_2 increases.

Table 2
Numerical determinations of $\overline{S}_{hx^*}$ due to making the variation in the Schmidt number S_c and solutal relaxation coefficient χ_2.

S_c	χ_2	$\overline{S}_{hx^*}$
0.1	0.1	0.4042
0.2		0.4762
0.3		0.5468
	0.2	0.4041
	0.3	0.4041
	0.4	0.4040

Table 3
Comparing the results of skin friction $\overline{C}_{f^*}$ by varying the inputs of Williamson coefficient.

W_e	Nadeem et al. [1]	Present Study
0	1	1
0.1	0.976588	0.9765
0.2	0.939817	0.9398
0.3	0.88272	0.8827

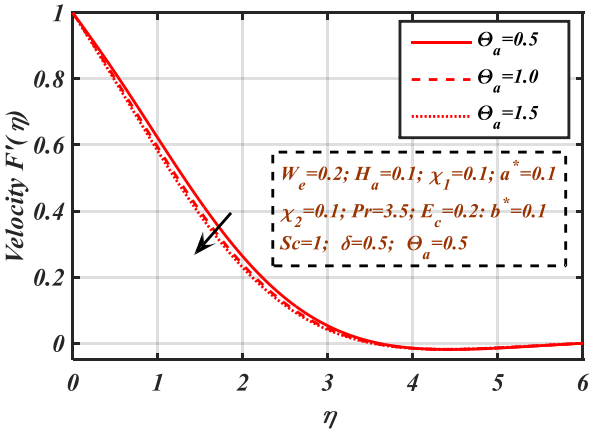

(2a): Sketch of Θ_a on $F'(\eta)$.

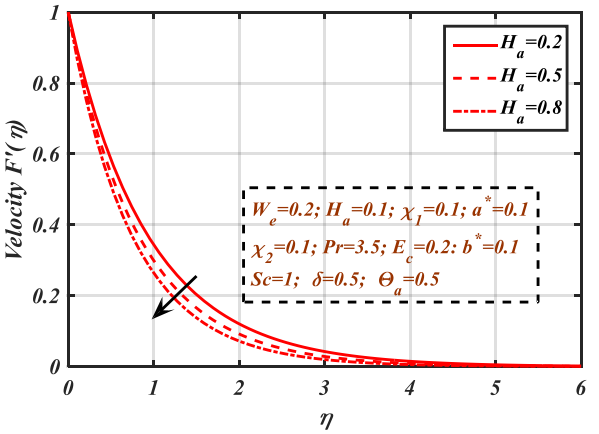

(2b): Sketch of H_a on $F'(\eta)$.

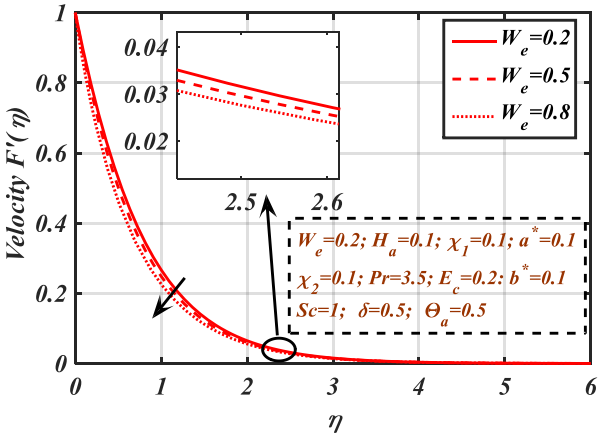

(2c): Sketch of W_e on $F'(\eta)$.

Fig. 2. a Sketch of Θ_a on $F^{'}(\eta)$.
Fig. (2b): Sketch of H_a on $F^{'}(\eta)$.
Fig. (2c): Sketch of W_e on $F^{'}(\eta)$.

Physically, the fluid needs more time to transfer mass rate because the stronger impact of χ_2, governs the transference of energy waves in a particular medium. Consequently, the fluid mass drops as the relaxation parameter upsurges. The graphical significance of reaction coefficient δ on the concentration regions are placed in Fig. (4c). The impression shows the declining behaviour of reaction coefficient on the concentration curve.

4.5. Graphical outcomes of Nusselt number $\overline{N}_{ux^*}$ and Sherwood number $\overline{S}_{hx^*}$

Fig. 5(a–c) are plotted to investigate the graphical behaviours of Nusselt and Sherwood numbers by making the variation in the Hartmann number H_a, Eckert number E_c, thermal relaxation coefficient χ_1 and reaction coefficient δ. The results of magnetic field parameter and Eckert number are shown in Fig. (5a). Both the parameters makes the decrement in the Nusselt number H_a. **The results of magnetic parameter and thermal relaxation coefficient are revealed in Fig. 5(b). The declining impact is noted by**

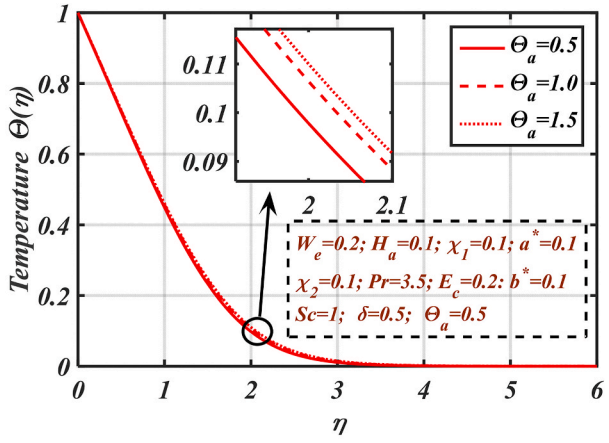

(3a): Sketch of Θ_a on $\Theta(\eta)$.

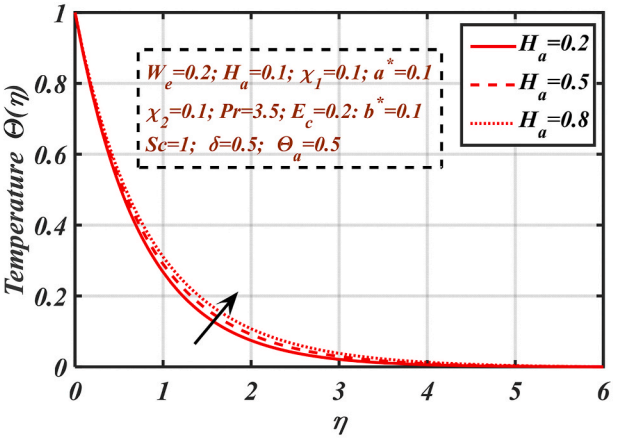

(3b): Sketch of H_a on $\Theta(\eta)$.

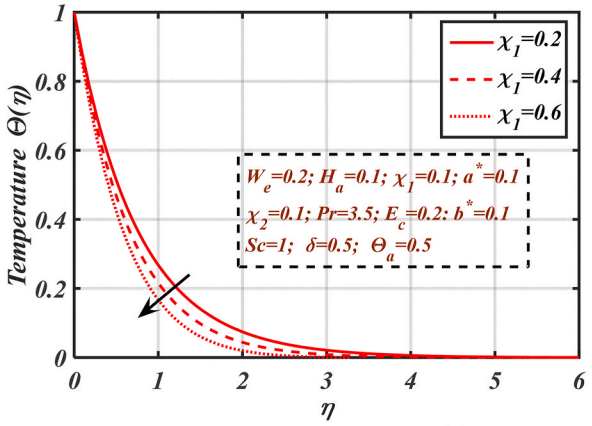

(3c): Sketch of χ_1 on $\Theta(\eta)$.

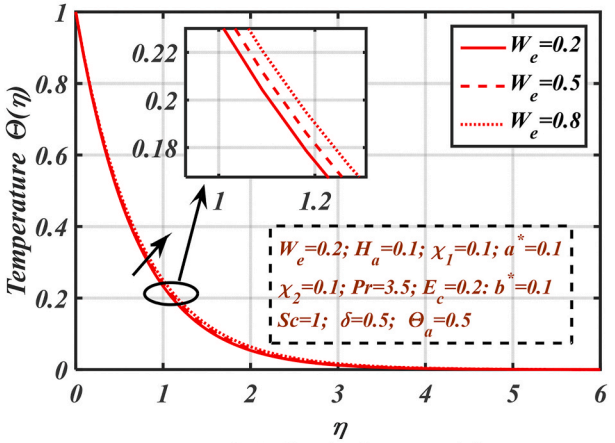

(3d): Sketch of W_e on $\Theta(\eta)$.

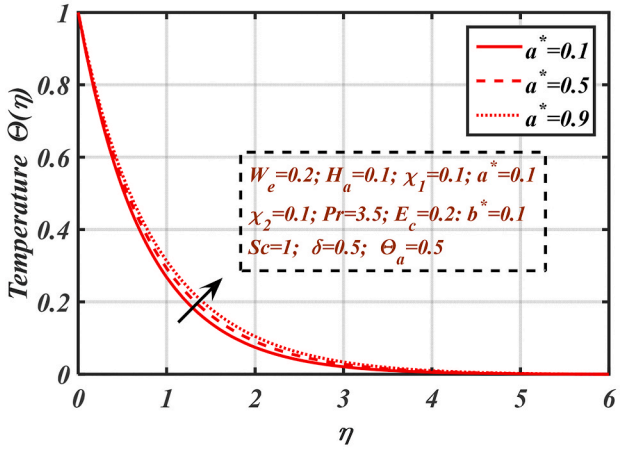

(3e): Sketch of a^* on $\Theta(\eta)$.

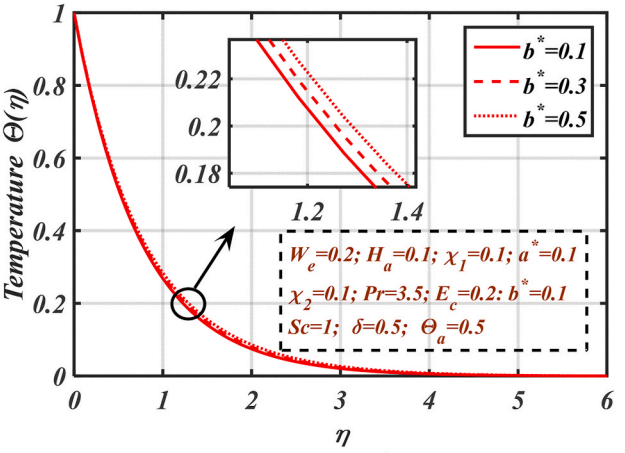

(3f): Sketch of b^* on $\Theta(\eta)$.

Fig. 3. a Sketch of Θ_a on $\Theta(\eta)$.
Fig. (3b): Sketch of H_a on $\Theta(\eta)$.
Fig. (3c): Sketch of χ_1 on $\Theta(\eta)$.
Fig. (3d): Sketch of W_e on $\Theta(\eta)$.
Fig. (3e): Sketch of a^* on $\Theta(\eta)$.
Fig. (3f): Sketch of b^* on $\Theta(\eta)$.

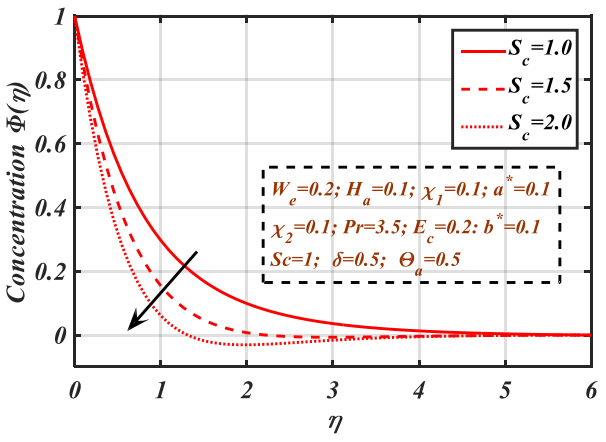

(4a): Sketch of S_c on $\Phi(\eta)$.

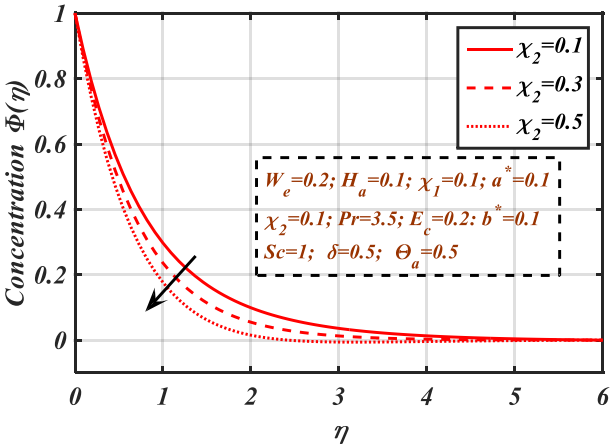

(4b): Sketch of χ_2 on $\Phi(\eta)$.

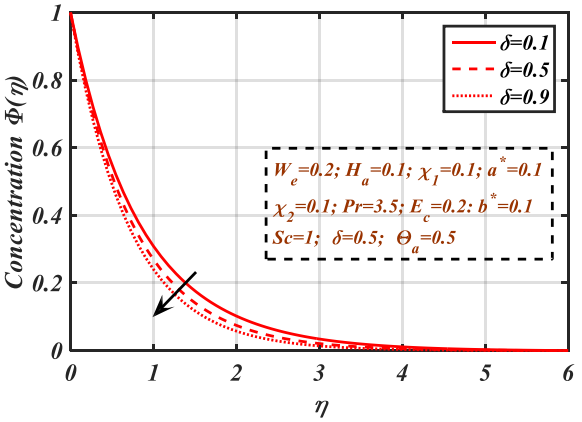

(4c): Sketch of δ on $\phi(\eta)$.

Fig. 4. a Sketch of S_c on $\Phi(\eta)$.
Fig. (4b): Sketch of χ_2 on $\Phi(\eta)$.
Fig. (4c): Sketch of δ on $\varphi(\eta)$..

producing the magnetic parameter and thermal relaxation coefficient. The sketch in Fig. (5c) reveals the graphical impression of Sherwood number $\overline{S}_{hx^*}$ by producing the reaction coefficient δ and Schmidt number S_c. **The finding indicates that the reaction coefficient δ and Schmidt number S_c makes the increment in the Sherwood number $\overline{S}_{hx^*}$.**

5. Conclusion

The purpose of conducting this problem is to determine the magnetohydrodynamic Williamson fluid with variable viscosity which is flowing on a stretchy surface. The mass and thermal transmission rates are analyzed by considering Joule heating, the Cattaneo-Christov model, heat source or sink, and chemical reaction. The findings of all these effects are listed here:

- The fluid motion decreases by producing the Weissenberg number and Hartmann number.
- The variable viscosity is the source of enhancement happening in the velocity and energy regions.
- The increasing magnitude of the Hartman number and Williamson fluid coefficient causes the energy flux to increase.
- By rising the Prandtl number and Schmidt number, the thermal and solutal field are decreased.
- The heat and solutal relaxation coefficients exhibit diminishing behaviour for the heat and mass distribution.
- The reaction coefficient caused the decrement in the concentration region.
- The decrements in results of Nusselt number are noted due to the Eckert number and magnetic field parameter whereas the thermal relaxation parameter makes the increment in Nusselt number.
- Both the chemical reaction and Schmidt number mark the increment in the Sherwood number.

There are several limitations and difficulties related to Williamson fluid flow on a stretching sheet, including the complexity of constitutive equations, nonlinearity, and numerical challenges. As the model equations are highly non-linear, we cannot find the exact

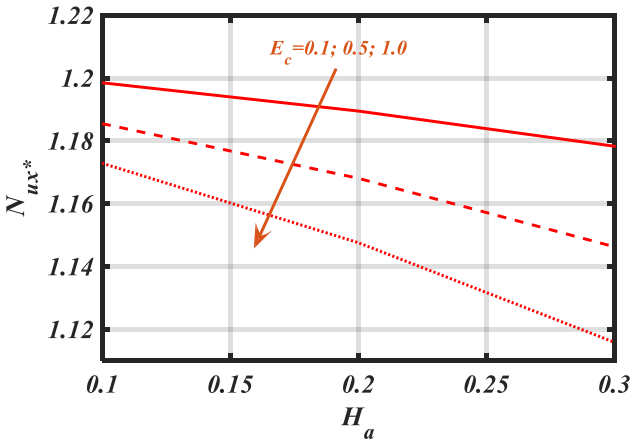

(a): Sketch of E_c on $\bar{N}_{ux^*}$.

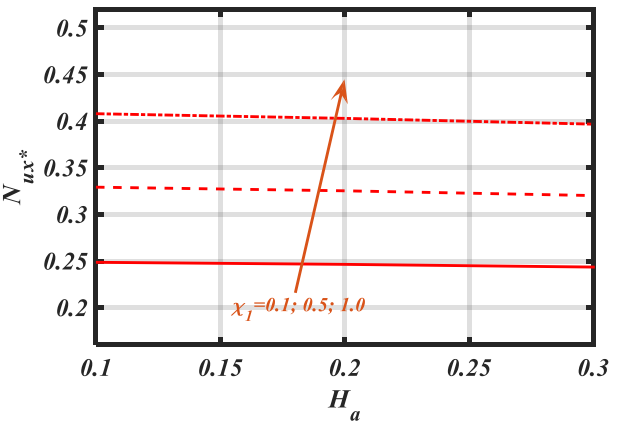

(b): Sketch of χ_1 on $\bar{N}_{ux^*}$.

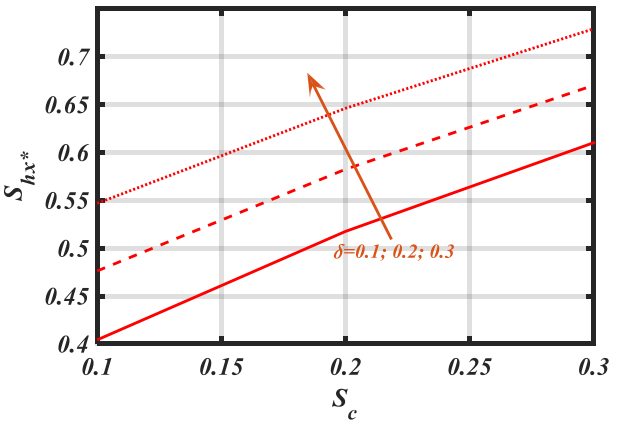

(c): Sketch of δ on $\bar{S}_{hx^*}$.

Fig. 5. (a)Sketch of E_c on $\overline{N}_{ux^*}$.
Fig. 5**(b):** Sketch of χ_1 on $\overline{N}_{ux^*}$.
Fig. 5**(c):** Sketch of δ on $\overline{S}_{hx^*}$.

solutions. To investigate the physical scenario, we cannot consider the fluid viscosity as a constant, therefore we must take variable viscosity.

We can further extend this work in the future by considering some other fluid models, such as Eyring-Powell fluid, Jeffery fluid, Sisko-fluid, Maxwell fluid, Carreau-Yaseuda fluid and power law fluids. To investigate the physical scenario, we can consider the fluid viscosity to be temperature dependent or space dependent. The thermal and solutal transfer rates are investigated by assuming the soret-dufour effects, bioconvection, nanofluids, hybrid nanofluids, viscous dissipation, and thermal radiation. This study is also extended further by assuming the variable thermal conduction and diffusion.

Funding statement

There is no funding statement for this manuscript.

Data availability statement

Data included in article are available anytime.

CRediT authorship contribution statement

T. Salahuddin: Visualization, Validation, Supervision. **Muhammad Awais:** Writing – review & editing, Writing – original draft, Visualization, Validation, Software, Resources, Methodology, Investigation, Formal analysis, Data curation, Conceptualization.

Declaration of competing interest

The authors declare that they have no known competing financial interests or personal relationships that could have appeared to influence the work reported in this paper.

Nomenclature

(x^*, y^*)	Cartesian coordinates (m)
(C^*, T^*)	concentration field and temperature field $\left(mol/m^3, k\right)$
p^*	Pressure (Pa)
(u^*, v^*)	components of velocity $\left(m/s\right)$
ρ	Density $\left(kg/m^3\right)$
(b_x^*, b_y^*)	Body forces
C_p	Specific heat $\left(J/kg\,K\right)$
τ^*	Stress tensor
(C_∞^*, T_∞^*)	upstream concentration and temperature $\left(mol/m^3, k\right)$
λ_2	Mass relaxation time
λ_1	Heat relaxation time
T_p^*	Variable surface temperature
K	Thermal conduction $\left(W/mK\right)$
Γ	Material constant
σ^*	Electrical conductivity $\left(S/m\right)$
C_p^*	Variable surface concentration
μ^*	Dynamic viscosity $\left(Ns/m^2\right)$
$B_\circ^*$	Magnetic field coefficient
D	Thermal diffusion $\left(m^2/s\right)$
κ	Reaction rate
(a^*, b^*)	Heat source/sink parameters
B	Stretching parameter
υ^*	Kinematic viscosity $\left(m^2/s\right)$
(Φ, Θ)	Dimensionless concentration and temperature variable
Θ_a	Viscosity coefficient
W_e	Weissenberg number
$F(\eta)$	Dimensionless velocity
H_a	Hartmann number
P_r	Prandtl number
χ_1	Thermal relaxation coefficient
E_c	Eckert number
δ	Reaction coefficient
χ_2	Solutal relaxation coefficient
S_c	Schmidt number
C_f	Skin friction
Re	Reynolds number

References

[1] S. Nadeem, S.T. Hussain, C. Lee, Flow of a Williamson fluid over a stretching sheet, Braz. J. Chem. Eng. 30 (2013) 619–625, https://doi.org/10.1590/S0104-66322013000300019.
[2] M.Y. Malik, T. Salahuddin, Numerical solution of MHD stagnation point flow of Williamson fluid model over a stretching cylinder, Int. J. Nonlinear Sci. Numer. Stimul. 16 (2015) 161–164, https://doi.org/10.1515/ijnsns-2014-0035.
[3] T. Salahuddin, M.A. Iqbal, A. Bano, M. Awais, S. Muhammad, Cattaneo-Christov heat and mass transmission of dissipated Williamson fluid with double stratification, Alex. Eng. J. 80 (2023) 553–558, https://doi.org/10.1016/j.aej.2023.09.012.
[4] M. Ramamoorthy, L. Pallavarapu, Radiation and Hall effects on a 3D flow of MHD Williamson fluid over a stretchable surface, Heat Transfer 49 (8) (2020) 4410–4426, https://doi.org/10.1002/htj.21833.
[5] K. Ahmed, W.A. Khan, T. Akbar, G. Rasool, S.O. Alharbi, I. Khan, Numerical investigation of mixed convective Williamson fluid flow over an exponentially stretching permeable curved surface, Fluids 6 (2021) 260, https://doi.org/10.3390/fluids6070260.

[6] M. Nawaz, M.A. Sadiq, Unsteady heat transfer enhancement in Williamson fluid in Darcy-Forchheimer porous medium under non-Fourier condition of heat flux, Case Stud. Therm. Eng. 28 (2021) 101647, https://doi.org/10.1016/j.csite.2021.101647.

[7] M. Waqas, M.I. Khan, Z. Asghar, S. Kadry, Y.M. Chu, W.A. Khan, Interaction of heat generation in nonlinear mixed/forced convective flow of Williamson fluid flow subject to generalized Fourier's and Fick's concept, J. Mater. Res. Technol. 9 (2020) 11080–11086, https://doi.org/10.1016/j.jmrt.2020.07.068.

[8] R. Meenakumari, P. Lakshminarayana, K. Vajravelu, Unsteady MHD flow of a Williamson nanofluid on a permeable stretching surface with radiation and chemical reaction effects, Eur. Phys. J. Spec. Top. 230 (2021) 1355–1370, https://doi.org/10.1140/epjs/s11734-021-00039-7.

[9] T. Salahuddin, Modelling unsteady waveform Williamson fluid flow near a permeable radioactive surface, Int. Commun. Heat Mass Tran. r 117 (2020) 104764, https://doi.org/10.1016/j.icheatmasstransfer.2020.104764.

[10] A. Hamid, Numerical study of temperature dependent thermal conductivity and homogeneous-heterogeneous reactions on Williamson fluid flow, Journal of Physics Communications 4 (2020) 085009, https://doi.org/10.1088/2399-6528/aba9f9.

[11] M. Awais, T. Salahuddin, Radiative magnetodydrodynamic cross fluid thermophysical model passing on parabola surface with activation energy, Ain Shams Eng. J. (2023) 102282, https://doi.org/10.1016/j.asej.2023.102282.

[12] B.N. Reddy, P. Maddileti, Casson nanofluid and Joule parameter effects on variable radiative flow of MHD stretching sheet, Partial Differential Equations in Applied Mathematics 7 (2023) 100487, https://doi.org/10.1016/j.padiff.2022.100487.

[13] M.D. Shamshuddin, S.U. Khan, O.A. Bég, T.A. Bég, Hall current, viscous and Joule heating effects on steady radiative 2-D magneto-power-law polymer dynamics from an exponentially stretching sheet with power-law slip velocity: a numerical study, Therm. Sci. Eng. Prog. 20 (2020) 100732, https://doi.org/10.1016/j.tsep.2020.100732.

[14] B.K. Swain, B.C. Parida, S. Kar, N. Senapati, Viscous dissipation and joule heating effect on MHD flow and heat transfer past a stretching sheet embedded in a porous medium, Heliyon 6 (10) (2020) e05338, https://doi.org/10.1016/j.heliyon.2020.e05338.

[15] B.K. Sharma, R. Gandhi, Combined effects of Joule heating and non-uniform heat source/sink on unsteady MHD mixed convective flow over a vertical stretching surface embedded in a Darcy-Forchheimer porous medium, Propulsion and Power Research 11 (2) (2022) 276–292, https://doi.org/10.1016/j.jppr.2022.06.001.

[16] S.A. Devi, M. Prakash, Temperature dependent viscosity and thermal conductivity effects on hydromagnetic flow over a slendering stretching sheet, Journal of the Nigerian Mathematical Society 34 (3) (2015) 318–330, https://doi.org/10.1016/j.jnnms.2015.07.002.

[17] E.O. Fatunmbi, A.S. Oke, S.O. Salawu, Magnetohydrodynamic micropolar nanofluid flow over a vertically elongating sheet containing gyrotactic microorganisms with temperature-dependent viscosity, Results in Materials (2023) 100453, https://doi.org/10.1016/j.rinma.2023.100453.

[18] M.G. Sobamowo, A.T. Akinshilo, Analysis of flow, heat transfer and entropy generation in a pipe conveying fourth grade fluid with temperature dependent viscosities and internal heat generation, J. Mol. Liq. 241 (2017) 188–198, https://doi.org/10.1016/j.molliq.2017.05.145.

[19] G.J. Reddy, M. Kumar, O.A. Beg, Effect of temperature dependent viscosity on entropy generation in transient viscoelastic polymeric fluid flow from an isothermal vertical plate, Phys. Stat. Mech. Appl. 510 (2018) 426–445, https://doi.org/10.1016/j.physa.2018.06.065.

[20] J.B.J. Fourier, Theorie Analytique De La Chaleur, 1822, https://doi.org/10.1017/CBO9780511693229. Paris.

[21] T. Hayat, A. Kiran, M. Imtiaz, A. Alsaedi, Cattaneo-Christov heat flux in flow by rotating disk with variable thickness, The European Physical Journal Plus 132 (2017) 1–18, https://doi.org/10.1140/epjp/i2017-11429-5.

[22] T. Salahuddin, Muhammad Awais, Cattaneo-Christov flow analysis of unsteady couple stress fluid with variable fluid properties: by using Adam's method, Alex. Eng. J. 81 (2023) 64–86, https://doi.org/10.1016/j.aej.2023.09.021.

[23] M. V. Reddy and P. Lakshminarayana, MHD radiative flow of Williamson nanofluid with Cattaneo-Christov model over a stretching sheet through a porous medium in the presence of chemical reaction and suction/injection, J. Porous Media, 25, https://doi.org/10.1615/JPorMedia.2022041423..

[24] M. Khan, A. Ahmed, M. Irfan, J. Ahmed, Analysis of Cattaneo–Christov theory for unsteady flow of Maxwell fluid over stretching cylinder, J. Therm. Anal. Calorim. 144 (2021) 145–154, https://doi.org/10.1007/s10973-020-09343-1.

[25] M. Awais, T. Salahuddin, Natural convection with variable fluid properties of couple stress fluid with Cattaneo-Christov model and enthalpy process, Heliyon 9 (8) (2023) e18546, https://doi.org/10.1016/j.heliyon.2023.e18546.

[26] T. Salahuddin, M. Awais, M. Khan, M. Altanji, Analysis of transport phenomenon in cross fluid using Cattaneo-Christov theory for heat and mass fluxes with variable viscosity, Int. Commun. Heat Mass Tran. 129 (2021) 105664, https://doi.org/10.1016/j.icheatmasstransfer.2021.105664.

[27] F.O.M. Mallawi, M. Bhuvaneswari, S. Sivasankaran, S. Eswaramoorthi, Impact of double-stratification on convective flow of a non-Newtonian liquid in a Riga plate with Cattaneo-Christov double-flux and thermal radiation, Ain Shams Eng. J. 12 (1) (2021) 969–981, https://doi.org/10.1016/j.asej.2020.04.010.

[28] M. Vinodkumar Reddy, G. Sucharitha, K. Vajravelu, P. Lakshminarayana, Convective flow of MHD non-Newtonian nanofluids on a chemically reacting porous sheet with Cattaneo-Christov double diffusion, Waves Random Complex Media (2022) 1–20, https://doi.org/10.1080/17455030.2022.2111478.

[29] T. humma, O.A. Bég, A. Kadir, Numerical study of heat source/sink effects on dissipative magnetic nanofluid flow from a non-linear inclined stretching/shrinking sheet, J. Mol. Liq. 232 (2017) 159–173, https://doi.org/10.1016/j.molliq.2017.02.032.

[30] U.S. Mahabaleshwar, K.N. Sneha, A. Chan, D. Zeidan, An effect of MHD fluid flow heat transfer using CNTs with thermal radiation and heat source/sink across a stretching/shrinking sheet, Int. Commun. Heat Mass Tran. 135 (2022) 106080, https://doi.org/10.1016/j.icheatmasstransfer.2022.106080.

[31] M. Ajaykumar, C.K. Ajay, A.H. Srinivasa, Effects of viscous dissipation, internal heat source/sink and Prandtl number on flow and heat transfer in a moving fluid over a moving flat surface with an applied magnetic field, in: Materials Today: Proceedings, 2023, https://doi.org/10.1016/j.matpr.2023.04.437.

[32] E. Ragupathi, D. Prakash, Role of linear and non-linear thermal radiation over the rotating porous disc with the occurrence of non-uniform heat source/sink: HAM analysis, Math. Comput. Simulat. (2023), https://doi.org/10.1016/j.matcom.2023.08.038.

[33] N.A.M. Noor, S. Shafie, Magnetohydrodynamics squeeze flow of sodium alginate-based Jeffrey hybrid nanofluid with heat sink or source, Case Stud. Therm. Eng. 49 (2023) 103303, https://doi.org/10.1016/j.csite.2023.103303.

[34] T. Salahuddin, M. Awais, W.F. Xia, Variable thermo-physical characteristics of Carreau fluid flow by means of stretchable paraboloid surface with activation energy and heat generation, Case Stud. Therm. Eng. 25 (2021) 100971, https://doi.org/10.1016/j.csite.2021.100971.

[35] T. Salahuddin, M. Awais, Z. Salleh, A flow study of Carreau fluid near the boundary layer region of paraboloid surface with viscous dissipation and variable fluid properties, J. Mater. Res. Technol. 14 (2021) 901–909, https://doi.org/10.1016/j.jmrt.2021.06.103.

[36] T. Salahuddin, M. Awais, A comparative study of Cross and Carreau fluid models having variable fluid characteristics, Int. Commun. Heat Mass Tran. 139 (2022) 106431, https://doi.org/10.1016/j.icheatmasstransfer.2022.106431.

[37] A.K. Pandey, S. Rajput, K. Bhattacharyya, A.J. Chamkha, D. Yadav, Potential impacts of Cattaneo–Christov model of heat flux on the flow of Carreau–Yasuda fluid with mixed convection over a vertical stationary flat plate, Forces in Mechanics 11 (2023) 100179, https://doi.org/10.1016/j.finmec.2023.100179.

[38] M.B. Ashraf, A. Tanveer, S. Ul haq, Effects of Cattaneo-Christov heat flux on MHD Jeffery nano fluid flow past a stretching cylinder, J. Magn. Magn Mater. 565 (2023) 170154, https://doi.org/10.1016/j.jmmm.2022.170154.

[39] T. Salahuddin, R. Ali, M. Khan, M. Awais, An axisymmetric flow analysis by means of tangent hyperbolic fluid with Cattaneo-Christov heat and mass flux model, J. Indian Chem. Soc. 99 (10) (2022) 100592, https://doi.org/10.1016/j.jics.2022.100592.

[40] S. Bilal, M.I. Shah, N.Z. Khan, A. Akgül, K.S. Nisar, Onset about non-isothermal flow of Williamson liquid over exponential surface by computing numerical simulation in perspective of Cattaneo Christov heat flux theory, Alex. Eng. J. 61 (8) (2022) 6139–6150, https://doi.org/10.1016/j.aej.2021.11.038.

[41] A. Dadheech, A. Parmar, K. Agrawal, Q. Al-Mdallal, S. Sharma, Second law analysis for MHD slip flow for Williamson fluid over a vertical plate with Cattaneo-Christov heat flux, Case Stud. Therm. Eng. 33 (2022) 101931, https://doi.org/10.1016/j.csite.2022.101931.

[42] A.A. Hakeem, N.V. Ganesh, B. Ganga, Effect of heat radiation in a Walter's liquid B fluid over a stretching sheet with non-uniform heat source/sink and elastic deformation, Journal of King Saud University-Engineering Sciences 26 (2) (2014) 168–175, https://doi.org/10.1016/j.jksues.2013.05.006.

[43] Z. Ullah, A. Abbas, E.R. El-Zahar, L.F. Seddek, A. Akgul, A.M. Hassan, Significance of thermal density and viscous dissipation on heat and mass transfer of chemically reactive nanofluid flow along stretching sheet under magnetic field, Results in Engineering (2023) 101413, https://doi.org/10.1016/j.rineng.2023.101413.

[44] A.B. Vishalakshi, U.S. Mahabaleshwar, M.H. Ahmadi, M. Sharifpur, An MHD Casson fluid flow past a porous stretching sheet with threshold Non-Fourier heat flux model, Alex. Eng. J. 69 (2023) 727–737, https://doi.org/10.1016/j.aej.2023.01.037.
[45] M.M. Rashidi, S. Bagheri, E. Momoniat, N. Freidoonimehr, Entropy analysis of convective MHD flow of third grade non-Newtonian fluid over a stretching sheet, Ain Shams Eng. J. 8 (1) (2017) 77–85, https://doi.org/10.1016/j.asej.2015.08.012.
[46] J.R. Reddy, J.R. Kumar, K.A. Sugunamma, N. Sandeep, Effect of cross diffusion on MHD non-Newtonian fluids flow past a stretching sheet with non-uniform heat source/sink: a comparative study, Alex. Eng. J. 57 (3) (2018) 1829–1838, https://doi.org/10.1016/j.aej.2017.03.008.